Diagnostics of model numerical cores: a model hierarchy

Nils P. Wedi

ECMWF, Shinfield Park, Reading
RG2 9AX, United Kingdom
wedi@ecmwf.int

ABSTRACT

This paper reviews a hierarchy of reduced models that assess the accuracy of numerical techniques as well as diagnose systematic errors of model dynamical cores. In the context of numerical weather prediction and climate research, dynamical and numerical aspects are often assessed using shallow-water models and idealised model "climate" simulations. Physical parametrizations and dynamics-physics interactions and their verification are commonly tested with models, ranging from single-column models (SCMs) to limited-area, large-eddy (LES) simulations. It is shown that reduced-size planet simulations, aquaplanets, and direct numerical simulations (DNS) of laboratory experiments complement such a hierarchy of reduced models, in particular for an assessment of the model behaviour in the horizontal resolution range $\Delta x = \mathcal{O}(0.1-20)$ km. The strategy of reductionism is shown to expose systematic errors of model dynamical cores, while testing their accuracy in canonical flow situations. Moreover, by isolating particular flow phenomena, tools are provided to improve the general understanding of global-scale climate models with growing complexity.

1 Introduction

The dynamical core is an important element of every atmosphere or ocean model. Historically, in the context of numerical weather prediction and climate research, the dynamical core is the (dry) part of the model without any diabatic forcings (i.e. physics). However, with resolutions ranging from $\Delta x = \mathcal{O}(0.1-20)$ km many processes that were traditionally computed in the "physics" (e.g. gravity wave drag, convection, moist processes, boundary layer turbulence), are partially or fully resolved and it becomes increasingly ambiguous if a parametrized (subgrid-scale) term should be computed at all, with subsequent implications for the dynamics-physics interface of the model. Hence, now and in the future it is not straight forward to assess the veracity of global-scale simulations with the full complexity of all modelled processes, as model design as well as physical parametrizations fundamentally change across the full range of resolutions that are becoming computationally affordable.

A practical strategy is therefore to use reduced models for diagnostic purposes. Here it is assumed that the essential flow characteristics remain unchanged when the domain, the forcings or the equations are changed. Although a complete physical similarity is precluded, an approximate dynamic similarity can be of practical importance; see section 10 in Buckingham (1914) and Wedi and Smolarkiewicz (2009a).

The shallow-water model represents an early example of such a reduced model. Taylor (1936) was the first to point out that the global atmosphere may be viewed as an infinite set of shallow-water layers, each representing a single mode of the full system. This aspect has been extensively used to test the numerical accuracy of different dynamical cores (Williamson et al., 1992), but also to analyse the dynamic behaviour of weather and climate (Matsuno, 1966; Lorenz, 1972; Hoskins, 1973). An example for both aspects will be given in section 2.1.

An alternative diagnostic strategy can be exploited for the 3D global atmosphere, where the planetary radius is suitably reduced to capture nonhydrostatic phenomena without incurring the computational

cost of actual simulations of weather and climate at nonhydrostatic resolution $\Delta x \leq \mathcal{O}(2)$ km. (Smolarkiewicz et al., 1999; Wedi and Smolarkiewicz, 2009a). In other words, the size of the computational domain is reduced without changing the depth or the vertical structure of the atmosphere. Here the underlying assumption is that the essential flow characteristics remain unchanged when the separation of horizontal and vertical scales is reduced (Kuang et al., 2005). The examples in section 2.2 illustrate the utility of the testing strategy with distinct-scale problems of atmospheric dynamics relevant to weather and climate. In particular, Held-Suarez (dry) "climate" simulations (Held and Suarez, 1994) can be used in the reduced-radius framework to evaluate the influence of the dynamical core formulation on an idealised climate state on a sphere, while the relative importance of individual terms in the equations is shifted with decreasing radii and/or increased rotation rate.

The next level of complexity in the hierarchy of models are aquaplanet simulations. In these global simulations with an underlying flat sea surface the model is forced by a family of latitudinal/longitudinal sea-surface temperature (SST) distributions and prescribed external forcings. In this case the models consist of the dynamical core and the physical parametrizations of radiation, boundary layer turbulence, convection and clouds. The Aquaplanet Intercomparison project (APE) (Neale and Hoskins, 2000) documents the intercomparison of various models for given SST distributions in a forthcoming ATLAS (*http://www.met.reading.ac.uk/ mike/APE/atlas.html*). In section 2.3 some examples are shown for ECMWF's integrated forecasting system (IFS) model, which participated in APE.

Laboratory experiments that isolate particular flow structures have long been regarded as complementary tools for studying the behaviour of large scale geophysical fluids, such as the Earth's atmosphere. With increased computer power available, a direct numerical simulation (DNS) of a laboratory experiment provides perhaps the most stringent test for any dynamical core. DNS means here integrating the Navier-Stokes equations without any parametrizations resolving the fluid motion up to the Kolmogorov length scale $\eta = (\nu^3/\varepsilon)^{1/4}$, where ν is the kinematic viscosity and ε denotes the kinetic energy dissipation rate. In this case grid sizes are $\Delta x = \mathcal{O}(\eta)$; see Moin and Mahesh (1998) for a review of DNS. In section 2.4 the laboratory experiment of Plumb and McEwan (1978), a canonical example of the influence of smaller-scale fluctuations on the large-scale flow, and the DNS thereof (Wedi and Smolarkiewicz, 2006) serve as an example. However, even large-eddy simulations (LES) of the global atmosphere are still out of reach. Instead, "virtual" laboratory experiments and large-eddy simulations (LES) thereof are emerging, in an attempt to explain the essence of particular flow phenomena that are a distinct multi-scale feature of the global atmosphere (Wedi and Smolarkiewicz, 2009b). The understanding of multi-scale phenomena — such as the Madden-Julian oscillation (MJO) — appear to be an important aspect for the design of future global numerical weather prediction (NWP) and climate models.

2 A hierarchy of reduced models

2.1 The shallow water model

As pointed out in the introduction, the early works of Taylor (1936) justify the use of a single layer equation set as a reduced model on the sphere. Therefore, it also often represents the first step in the development of a new dynamical core. The nonlinear shallow water equations on the sphere may be written as

$$\begin{aligned} &\frac{\partial \zeta}{\partial t} + \nabla \cdot (\zeta + f)\mathbf{v}_h = -K\nabla^4 \zeta \\ &\frac{\partial \delta}{\partial t} - \mathbf{k} \cdot \nabla \times (\zeta + f)\mathbf{v}_h + \nabla^2 (gH + 0.5\mathbf{v}_h \cdot \mathbf{v}_h) = -K\nabla^4 \delta \\ &\frac{dh}{dt} + h\delta = 0 \end{aligned} \tag{1}$$

where $\zeta \equiv \mathbf{k} \cdot (\nabla \times \mathbf{v}_h)$ denotes relative vorticity and $\delta \equiv \nabla \cdot \mathbf{v}_h$ is the horizontal divergence with horizontal velocity vector $\mathbf{v}_h$; h denotes the shallow water depth, $H = h + h_s$ is the shallow water height above the orography h_s, and f and g symbolise the 'Coriolis parameter' and gravity (both vertically oriented); see Williamson et al. (1992) for alternative forms of the equations and in particular explicit forms of the spherical horizontal gradient operator ∇ and the Laplacian ∇^2. The equations in (1) are in particular useful in the context of spectral models such as IFS, where the Laplacian is readily available. In IFS, the total derivative d/dt is evaluated along a semi-Lagrangian trajectory (Ritchie, 1988; Temperton et al., 2001). The ∇^4 diffusion terms that are used in the discretised version of IFS (and likewise in the operational forecast model) have been added for completeness, to obtain results as close as possible to the operational NWP model.

The first example — test case 1 in Williamson et al. (1992) — illustrates its use for diagnosing the accuracy of advection of the discretised equations by simulating the advection of a cosine-bell-shaped hill over the pole. Diagnostic error measures plotted as a function of time or as a function of resolution for example for the depth h are defined as

$$\begin{aligned} I_1(h) &:= \frac{I[|h(\lambda,\theta) - h_T(\lambda,\theta)|]}{I[|h_T(\lambda,\theta)|]} \\ I_2(h) &:= \frac{\sqrt{I[(h(\lambda,\theta) - h_T(\lambda,\theta))^2]}}{\sqrt{I[h_T(\lambda,\theta)^2]}} \\ I_\infty(h) &:= \frac{max_{\lambda,\theta}|h(\lambda,\theta) - h_T(\lambda,\theta)|}{max_{\lambda,\theta}|h_T(\lambda,\theta)|}, \end{aligned} \tag{2}$$

where I denotes the discrete approximation to the global integral $I(h) = \frac{1}{4\pi}\int_0^{2\pi}\int_{-\pi/2}^{\pi/2} h(\lambda,\theta)\cos\theta d\theta d\lambda$ and (λ,θ) are longitude and latitude, respectively. The value h_T denotes the true solution, which in this particular test case is given as the initial condition after 12 days of integration or one full rotation of the hill around the sphere. A recent example of the error measures in (2) for this test case can be found in Thomas and Loft (2002). Figure 1 shows the result of the shallow water version of IFS after one rotation of the hill over both poles. The magnitude of the deviation (panel c), obtained with the resolution and settings of ERA40 (Uppala et al., 2005), gives a magnitude of the I_∞ error that is approximately one order of magnitude larger than the values obtained with the spectral element model in Thomas and Loft (2002).

The second example illustrates the dynamic behaviour of weather and climate by means of the shallow-water model, showing the influence of the lunar gravitational potential on the stability of the Rossby-Haurwitz wave. Rossby-Haurwitz waves as depicted in Panel a of Fig. 2 are steadily propagating solutions of the fully nonlinear nondivergent barotropic vorticity equation on the sphere (Haurwitz, 1940). For the shallow-water equations on the sphere, an analytically prescribed Rossby-Haurwitz wave initial condition is expected to evolve similarly steady as with the barotropic vorticity equation (Thuburn and Li, 2000). However, Rossby-Haurwitz waves with wavenumbers ≥ 4 have been found to be unstable to small perturbations, suggesting a limit to the predictability of weather (Lorenz, 1972; Hoskins, 1973; Thuburn and Li, 2000). While in Thuburn and Li (2000) the emphasis is on numerically generated perturbations, here we review the influence of small but persistent extra-terrestrial forces, such as the gravitational pull of the moon. The gravitational acceleration provided by the moon adds rhs forcing terms in the momentum equation of the form $-\nabla\Omega_{tidal}$, with the lunar potential Ω_{tidal} defined by geometrical/astronomical considerations, cf. Chapman and Lindzen (1970), p.121-123 for details.

The result of the IFS simulations after 200 days of simulation without (panel a) and with the influence of the lunar gravitational potential are shown in Fig. 2. The Rossby-Haurwitz wave with wavenumber 4 is extremely stable for the IFS spectral shallow water model, whereas the lunar gravitational potential destabilises the flow after about 100 days with a resulting substantial cross polar flow, variations of high and low pressure systems and their corresponding jets, cf. panel b in Fig. 2. Interestingly, even

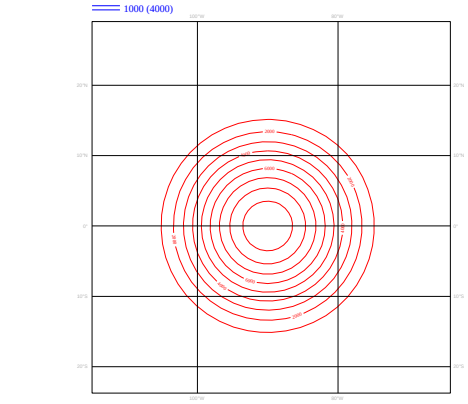

a

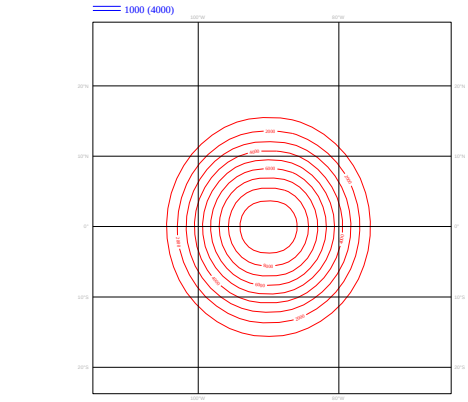

b

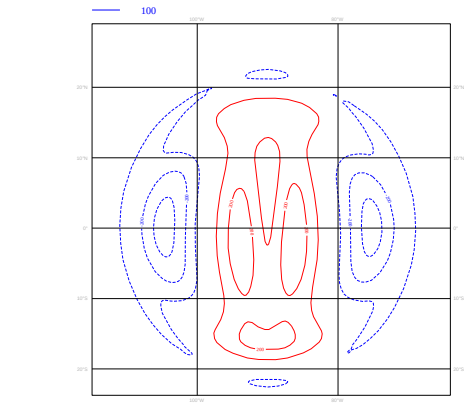

c

Figure 1: Panel a shows the initial geopotential of a cosine-bell-shaped hill (test case 1 in Williamson et al. (1992)) with a 1000 *m centre height of the hill* h_s*. Panel b shows the result of the IFS simulation after 12 days or one full rotation in north-south direction over both poles* ($\alpha = 90$ *degrees), and panel c shows the difference in geopotential height.*

a

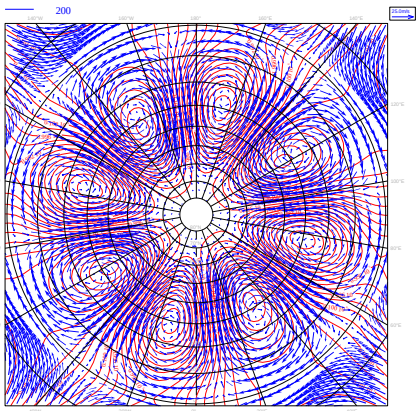

b

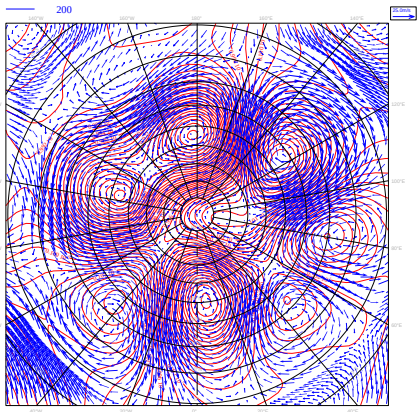

Figure 2: Geopotential and wind vectors are shown of a propagating Rossby-Haurwitz wave as viewed from the North Pole from simulations of the IFS shallow-water model without (panel a) and with (panel b) the influence of the gravitational pull of the moon.

the Rossby-Haurwitz wave with wavenumber 3 is destabilised in this manner (not shown), suggesting a decisive influence of the lunar potential on the long-range behaviour of large-scale atmospheric waves. So does the lunar gravitational pull matter for medium-range weather forecasts of the atmosphere ? It appears not. Figure 3 shows the spatial standard deviation of the forecast difference, cf. Jung and Vitart (2005) for details, of the 200hPa geopotential height surface for two sets of 31 forecasts using the full ECMWF IFS model with T_L255 resolution and 91 vertical levels, with and without lunar forcing, respectively. The figure indicates that there is no advantage adding the lunar forcing over a random single point perturbation. Nevertheless, on this basis it would be interesting to examine the value of adding the gravitational potential of the moon to seasonal forecasts in the future.

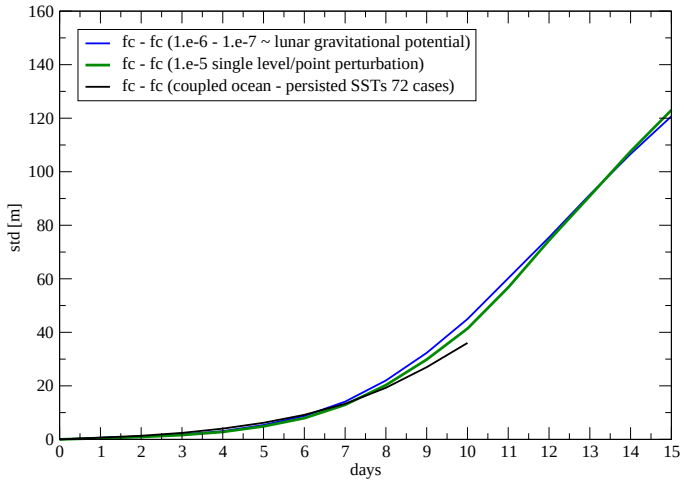

Figure 3: Spatial standard deviation (std) of the forecast difference of the 200hPa geopotential height surface between two sets of 31 forecasts without and with the lunar forcing included. As a reference the std of the forecast difference with a set of forecasts using random single point perturbations, and the std of using/not using a coupled ocean model (Jung and Vitart, 2005).

The example of the influence of the lunar potential provides a methodology to diagnose the influence of small perturbations on the short- and medium-range forecast. Moreover, it suggests that perturbations of similar magnitude in the momentum equations — e.g. the vertical acceleration of the Coriolis force as introduced by relaxing the shallow atmosphere approximation — are also likely to be of minor importance to the medium-range forecast performance.

2.2 Idealised reduced-radius simulations on the sphere

With the emergence of non-hydrostatic global dynamical cores it is desirable to directly compare quantitatively and qualitatively with LES benchmarks of limited-area models and Cartesian-domain analytic solutions published in the literature. In the framework proposed in Wedi and Smolarkiewicz (2009a) the planetary radius is suitably reduced to capture nonhydrostatic phenomena without incurring the computational cost of actual simulations of weather and climate at nonhydrostatic resolution $\Delta x \leq \mathcal{O}(2)$ km. The usefulness of this testing strategy is illustrated in Wedi and Smolarkiewicz (2009a) and Wedi et al. (2009) with a series of canonical flow problems ranging from horizontally and vertically propagating spherical acoustic-waves, "local-scale" orographically forced gravity waves in the presence of shear and critical levels, to "global-scale" planetary Rossby waves in Held-Suarez simulations (Held and Suarez, 1994). The test cases were conducted for two very different global dynamical cores, where the results

of the nonhydrostatic global IFS were compared with numerical solutions of the multi-scale anelastic research code EULAG (Prusa et al., 2008). Despite their distinctively different development paths and theoretical/numerical features, both models are equivalently setup on the sphere.

The Held-Suarez setup consists of dynamical core simulations, where the effect of the physics is emulated by adding the frictional term $-k_{\mathbf{v}}\mathbf{v}$ on the rhs of the momentum equation and adding $-k_T(T-T_{eq})$ in the thermodynamic equation, where $k_{\mathbf{v}}, k_T$ denote frictional/heating coefficients and T_{eq} defines a zonally symmetric temperature distribution in terms of a meridional and a vertical temperature gradient, see Wedi and Smolarkiewicz (2009a) for details. Notably, if the Rossby number $Ro = U/fL$ — with U denoting a characteristic zonal velocity, $L \sim a$ denoting a characteristic length scale (here taken as the planetary radius a), and f is the Coriolis parameter — is kept constant, a reduction of the planetary radius a implies an increase in the rotation rate and, thus, a corresponding increase in the frictional/heating time factors that define the coefficients $k_{\mathbf{v}}, k_T$. The latter may be used to change the relative influence of individual terms in the equations and thus for example further explore the impact of the deep vs. shallow atmosphere approximation on the zonally averaged "climate" state, cf. Fig.18 in Wedi and Smolarkiewicz (2009a).

However, apart from comparisons of the zonal mean state of Held-Suarez simulations, there is substantial extratropical variability, two subtropical jets, and a simplified tropical regime — enforced by the prescribed meridional and vertical temperature gradients. The Held-Suarez setup thus may be used to explore aspects of the tropical-extratropical interaction in a simplified global atmospheric model without any elaborate physical parametrizations or moist processes involved. For example, panel a in Fig. 4 shows for EULAG the temporal anomaly of velocity potential at 600 hPa, often interpreted as the equivalent barotropic level, in a Hovmöller representation (meridionally averaged between ± 10 degrees). Panel b shows the corresponding temporal anomaly of velocity potential at 200 hPa, a tracer often used to identify intraseasonal oscillations such as the MJO. Panels c-d in Fig. 4 show the equivalent results for the IFS model. There are several (albeit very different between the two models) episodic temporal flow anomalies of divergent flow in 200 hPa (negative velocity potential in black contours) that match in time and location with convergent flow anomalies below in 600 hPa (positive velocity potential in white contours). A wavenumber frequency analysis of velocity potential for both models (not shown) exhibits dominant periods between 29 and 66 days for eastward wavenumber one. An analysis of the power spectra of re-analysis data from ERA40 zonal mean zonal wind[1] at 200hPa or at 500hPa also shows a statistically robust deviation from an artificially created red noise spectrum in the range 20-60 days (Wedi, 2004). Figure 5 shows a Hovmöller diagram of velocity potential anomalies retrieved from the ERA40 reanalysis at 600 hPa and at 200 hPa, respectively. A strong MJO event starting approximately on the 1st May 2002 can be identified as a slowly eastward propagating positive velocity potential anomaly in 600 hPa (white contours), and corresponding negative velocity potential (black contours) at 200 hPa, both similar in appearance to some of the episodic events occurring in the idealised Held-Suarez simulations. Preliminary results, which utilise the reduced-size planet framework to vary the Rossby number Ro, reveal that the amplitude and occurrence of the episodically occurring velocity potential anomalies are decreased with increasing Rossby number. A possible explanation of the quasi-barotropic behaviour of the large-scale anomalous tropical disturbances in the Held-Suarez simulations and their sensitivity to the Rossby number is discussed further in Wedi and Smolarkiewicz (2009b).

2.3 APE aquaplanet simulations

The next level of complexity in the hierarchy of models are aquaplanet simulations, which use the models' physical parametrizations of radiation, boundary layer turbulence, convection and clouds but simplify the full complexity of global simulations of weather and climate by removing the topography

[1] averaged between ± 10 degrees latitude over 35 years

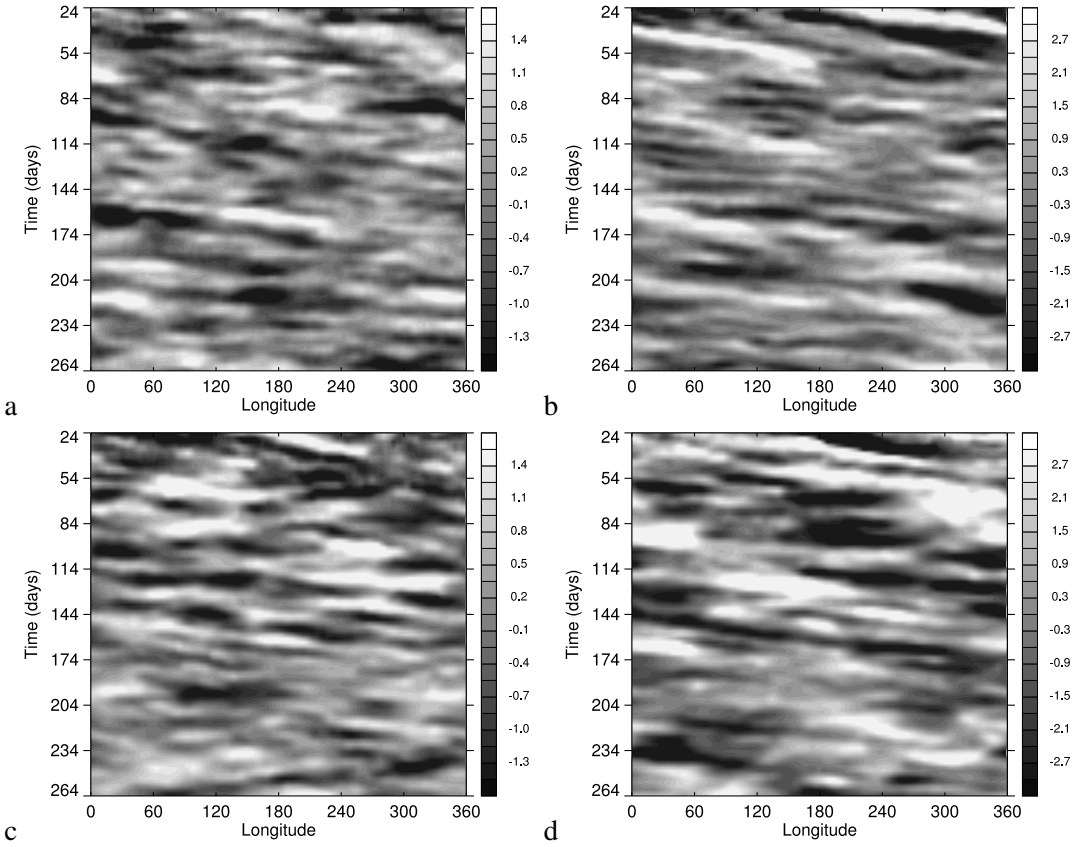

Figure 4: Hovmöller diagram of the temporal anomaly of velocity potential at 600 *hPa height (panel a) and the corresponding diagram at* 200 *hPa height (panel b) for the EULAG Held-Suarez simulation. Panels c - d are the equivalent figures for the IFS simulation. The data is meridionally averaged between* ± 10 *degrees, and for the EULAG model has been converted from its z-coordinate using the standard scale height* 7 *km.*

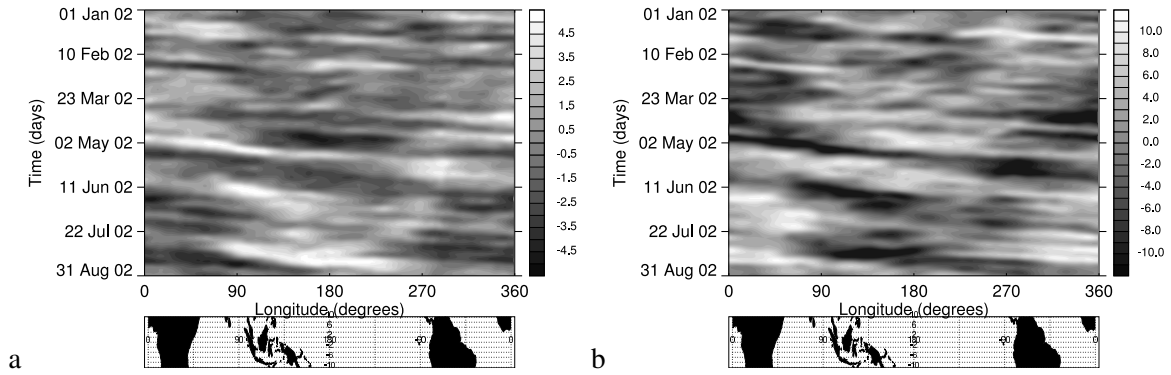

Figure 5: Hovmöller diagram of the temporal anomaly of velocity potential at 600 *hPa height (panel a) and the corresponding diagram at* 200 *hPa height (panel b) for the ERA40 re-analysis data. The data is meridionally averaged between* ± 10 *degrees. There is a strong MJO event starting approximately on 1st May 2002. The sketches below identify the continents.*

and continents. Instead, the model is forced by a prescribed SST distribution. Examples of zonally symmetric SST distributions (Neale and Hoskins, 2000) taken from the APE-Atlas are shown in Fig. 6. In these cases, the meridional gradients of the SSTs effectively initiate and enforce the ensuing global circulation.

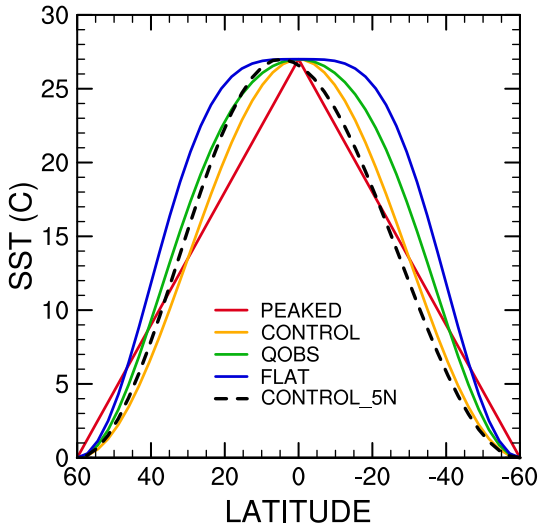

*Figure 6: Examples of the zonally symmetric SST distributions of the APE intercomparison project, taken from the APE-Atlas (*http://www.met.reading.ac.uk/ mike/APE/atlas.html*).*

When changes are made to the physical parametrizations, the aquaplanet setup can be useful to identify their impact on circulation changes more easily. For example, a prominent change of the convection parametrization occurred between the IFS model cycles CY29R2 and CY32R3, leading to a much improved representation of linear equatorial waves (Bechtold et al., 2008) and their respective signature on tropical precipitation as shown for IFS aquaplanet simulations with varying SST distributions in Fig. 7.

Moreover, the APE intercomparison revealed a large variety of organised convection and precipitation patterns between the different participating models (not shown). As the formation of organised convection is sensitive to the explicit or implicit viscosity in under-resolved simulations and in particular the anisotropy of viscosity (ie. horizontal vs. vertical) (Piotrowski et al., 2009), CONTROL SST aquaplanet simulations emerge as an excellent diagnostic tool to examine the influence of different formulations of global dynamical cores — and their implicit or explicit numerical diffusion — on the organisation of convection, an important aspect of future weather and climate predictions.

2.4 DNS or LES of laboratory experiments

DNSs or LESs of laboratory experiments represent a stringent challenge for model numerical cores. While a realistic simulation of a laboratory experiment does not necessarily guarantee that the same nu-

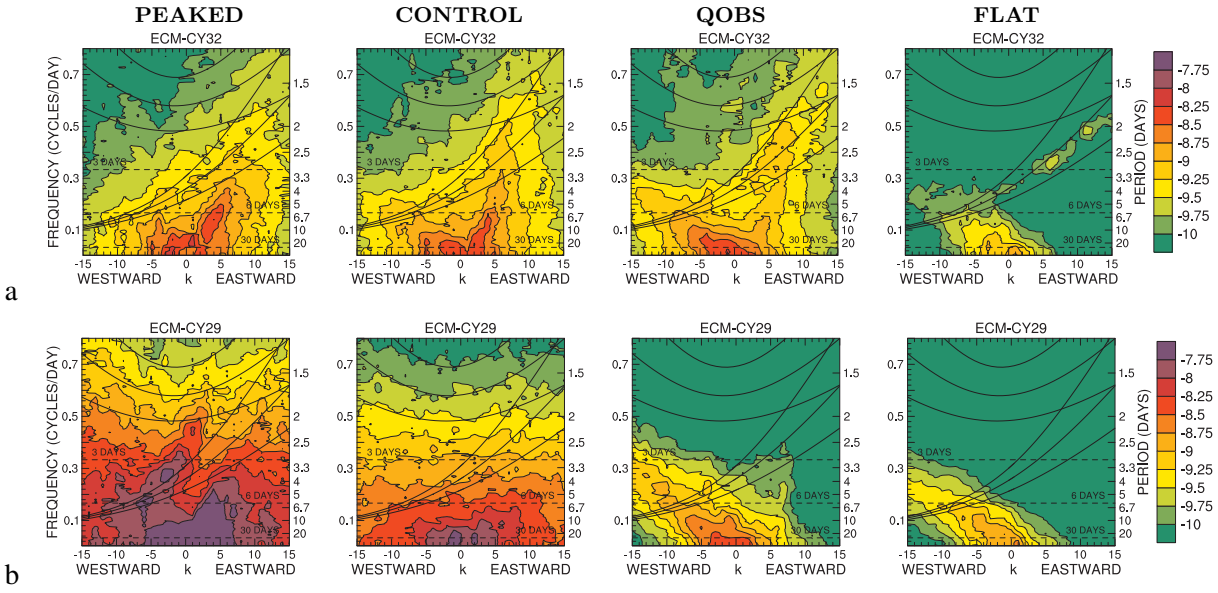

*Figure 7: Wavenumber frequency diagrams of log(power) of the symmetric modes of equatorial precipitation for the APE SST distributions PEAKED, CONTROL, QOBS and FLAT. Results are shown for the aquaplanet IFS simulations using cycle CY32R3 and CY29R2, respectively. The plots are taken from the APE-Atlas (*http://www.met.reading.ac.uk/ mike/APE/atlas.html*).*

merics perform well at global scales on the sphere, convergence in the the limit of gridsizes $\Delta x = \mathscr{O}(\eta)$ builds confidence in the overall numerical procedure. Moreover, with increasing resolution of weather and climate simulations it is relevant how the numerics of a model deals with the influence of small-scale fluctuations on the larger scale flow, when such mechanism is only partially or not at all parametrized. In particular, "virtual" laboratory setups provide another diagnostic tool to study the dynamics of selected flow phenomena, while examining the role of implicit or explicit dissipation. This has been demonstrated in the DNS of the laboratory experiment of Plumb and McEwan (Plumb and McEwan, 1978; Wedi and Smolarkiewicz, 2006), which represents a dynamical analogue to the quasi-biennial oscillation (QBO), the dominant variability in the equatorial stratosphere. The basic mechanism in the numerical simulations and the laboratory experiment is the sequence of gravity wave excitation by simple fluctuations of the upper or lower boundary, subsequent wave-wave mean flow interactions, critical layer formation followed by wave breaking and the emergence of a long-time zonal mean zonal flow oscillation, entirely driven by the wave momentum flux changes. All of these gravity wave processes and subsequent zonal mean flow changes are found in the atmosphere and hence the accuracy of different numerical choices for the simulation of wave-driven flow phenomena is relevant to weather and climate predictions.

For example, a comparison of the zonal mean zonal flow reversal in numerical simulations of the QBO analogue with a flux-form Eulerian and a semi-Lagrangian advection algorithm (Wedi, 2006) showed the onset of critical layers in different spatial positions for the latter, creating different bifurcation points for the flow development. Since in general flux-form schemes have higher-order truncation errors proportional to the differentials of fluxes of the primitive variables rather than to the differentials of the variables themselves (as characteristic of advective form schemes), the authors in Smolarkiewicz and Margolin (1997) concluded that the overall accuracy of the approximation increases when the fluxes of the variables exhibit a greater degree of homogeneity than the variables themselves. This may be the case in the QBO analogue simulations with fairly steady wave momentum fluxes below the critical layer. It is not clear, however, if in general higher resolution simulations are characterised by less homogeneity

of the prognostic variables compared to their associated fluxes.

It appears that with increased resolution — and lacking suitable parametrizations — the role of higher-order truncation errors of the numerical core itself gains importance, in particular also for the organisation of convection, as implied by the implicit LES (ILES) simulations in Piotrowski et al. (2009) and Wedi and Smolarkiewicz (2009b). For example, in the latter reference, large-scale anomalous solitary structures emerge in the simulations on an equatorial beta-plane when a translating and pulsating lateral forcing is applied at the meridional boundaries. When the boundary meander is stopped at $t^* = 762$, the solitary structures exhibit an extraordinary persistence (Wedi and Smolarkiewicz, 2009b). Panel a in Fig. 8 shows the result of a flux-form Eulerian simulation that has been restarted at $t^* = 762$ using the same flux-form Eulerian scheme, whereas panel b shows the result of the simulation restarted using a semi-Lagrangian scheme. Visibly the persistence and the solitary anomaly in velocity potential is lost, if the simulation is continued with the semi-Lagrangian scheme. The results imply a decisive influence of the numerical model core on the formation and the persistence of temporal flow anomalies, which is consistent with the large discrepancies found in the previously described APE intercomparison for temporal anomalies of precipitation (David Williamson, personal communication).

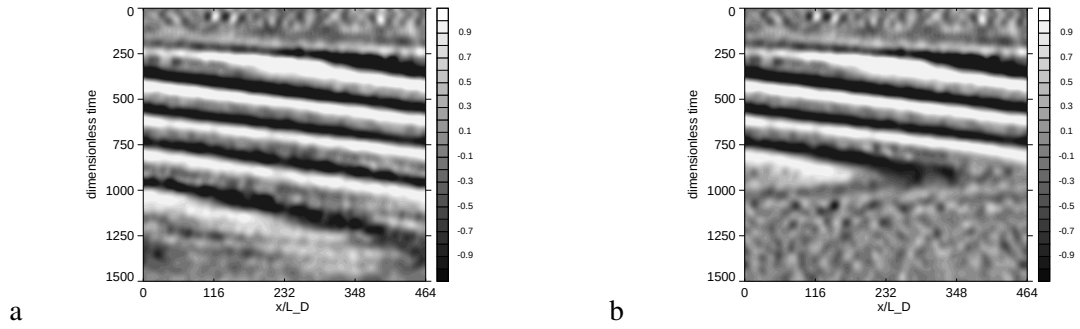

Figure 8: Hovmöller diagrams of the temporal anomaly of velocity potential ($\times 10^{-5}\ m^2 s^{-1}$) for the simulation of a stably stratified flow with uniform bottom heating and boundary layer friction at the bottom and the lateral walls of an equatorial beta plane. Panel a shows the simulation result with a flux-form Eulerian scheme, where the lateral boundary oscillation has been stopped at $t^* = 762$ and the model restarted. Panel b shows the simulation result when the model is continued using a semi-Lagrangian scheme. Note that the data displayed in panel a and b is identical upto $t^* = 762$. The Hovmöller data has been averaged over the near equatorial region $\pm 0.844 L_D$ from the mid-channel and lowpass filtered, to attenuate all frequencies larger and equal to the beat frequency of the boundary oscillation. Both time and the zonal length are nondimensionalised using the internal Rossby radius of deformation L_D; see Wedi and Smolarkiewicz (2009b) for details.

3 Conclusion

The diagnostic concept of reductionism has been introduced with a hierarchy of examples with gradually increasing complexity — ranging from a shallow water model, reduced-size planet, Held-Suarez and aquaplanet simulations, to DNS and LES of real or "virtual" laboratory experiments. The testing strategy has been shown to be useful for evaluating numerical or systematic errors for canonical flow situations. However, even more so the hierarchy of diagnostic tools provided (especially when applied within the same numerical modelling framework) aims to narrow the widening gap between the theoretical understanding of the Earth's climate system and the growing complexity of comprehensive global-scale climate simulations (Held, 2005).

Acknowledgements

I am grateful to Piotr Smolarkiewicz for many useful discussions. Furthermore, I would like to thank Mike Blackburn and Dave Williamson for their permission to show figures from the APE-Atlas that is currently in preparation, and I would like to thank Thomas Jung for his help in creating Figure 3. Finally, I am grateful to Martin Miller for his comments on an earlier version of the manuscript.

References

Bechtold, P., M. Koehler, T. Jung, F. Doblas-Reyes, M. Leutbecher, M. J. Rodwell, F. Vitart, and G. Balsamo (2008). Advances in simulating atmospheric variability with the ecmwf model: from synoptic to decadal time-scales. *Q.J.R. Meteorol. Soc. 134*, 1337–1351.

Buckingham, E. (1914). On physically similar systems; illustrations of the use of dimensional equations. *Physical Review 4*(4), 345–376.

Chapman, S. and R. S. Lindzen (1970). *Atmospheric Tides*. Dordrecht, Holland: Reidel Publishing Company.

Haurwitz, B. (1940). The motion of the atmospheric disturbances on a spherical earth. *J. Marine Res. 3*, 254–267.

Held, I. (2005). The gap between simulation and understanding in climate modelling. *Bull. Am. Meteor. Soc. 86*, 1609–1614.

Held, I. and M. Suarez (1994). A proposal for the intercomparison of the dynamical cores of atmospheric general circulation models. *Bull. Am. Meteorol. Soc. 73*, 1825–1830.

Hoskins, B. J. (1973). Stability of the Rossby-Haurwitz wave. *Q.J.R. Meteorol. Soc. 99*, 723–745.

Jung, T. and F. Vitart (2005). Short-range and medium-range weather forecasting in the extratropics during wintertime with and without an interactive ocean. *Mon. Weather Rev. 134*, 1972–1986.

Kuang, Z., P. Blossey, and C. Bretherton (2005). A new approach for 3d cloud-resolving simulations of large-scale atmospheric circulation. *Geophys. Res. Lett. 32*(L02809), 1–4.

Lorenz, E. D. (1972). Barotropic instability of Rossby wave motion. *J. Atmos. Sci. 29*, 258–264.

Matsuno, T. (1966). Quasi-geostrophic motions in the equatorial area. *J. Meteor. Soc. Japan 44*, 25–43.

Moin, P. and K. Mahesh (1998). Direct numerical simulation: A tool in turbulence research. *Annu. Rev. Fluid Mech. 30*, 539–578.

Neale, R. B. and B. J. Hoskins (2000). A standard test for AGCMs and their physical parameterizations. I: The proposal. *Atmos. Sci. Letters 1*, 101–107.

Piotrowski, Z. P., P. K. Smolarkiewicz, S. P. Malinowski, and A. Wyszogrodzki (2009). On numerical realizability of thermal convection. *J. Comput. Phys. 228*, 6268–6290.

Plumb, R. A. and D. McEwan (1978). The instability of a forced standing wave in a viscous stratified fluid: A laboratory analogue of the quasi-biennial oscillation. *J. Atmos. Sci. 35*, 1827–1839.

Prusa, J. M., P. K. Smolarkiewicz, and A. A. Wyszogrodzki (2008). EULAG, a computational model for multiscale flows. *Comput. Fluids 37*, 1193–1207.

Ritchie, H. (1988). Application of the semi-Lagrangian method to a spectral model of the shallow water equations. *Mon. Weather Rev. 116*, 1587–1598.

Smolarkiewicz, P. K., V. Grubišić, L. G. Margolin, and A. A. Wyszogrodzki (1999). Forward-in-time differencing for fluids: Nonhydrostatic modelling of fluid motions on a sphere. Proc. 1998 Seminar on Recent Developments in Numerical Methods for Atmospheric Modelling, Reading, UK, pp. 21–43. Eur. Cent. For Medium-Range Weather Forecasts.

Smolarkiewicz, P. K. and L. G. Margolin (1997). On forward-in-time differencing for fluids: An Eulerian/semi-Lagrangian non-hydrostatic model for stratified flows. *Atmos. Ocean Special 35*, 127–152.

Taylor, G. I. (1936). The oscillations of the atmosphere. *Proc. Roy. Soc. London A 156*(888), 318–326.

Temperton, C., M. Hortal, and A. Simmons (2001). A two-time-level semi-Lagrangian global spectral model. *Q.J.R. Meteorol. Soc. 127*, 111–127.

Thomas, S. J. and R. D. Loft (2002). Semi-implicit spectral element atmospheric model. *J. Sci. Comput. 17*, 339–350.

Thuburn, J. and Y. Li (2000). Numerical simulations of Rossby-Haurwitz waves. *Tellus 52 A*, 181–189.

Uppala, S. M., P. W. Kallberg, A. J. Simmons, U. Andrae, V. da Costa Bechtold, M. Fiorino, J. K. Gibson, J. Haseler, A. Hernandez, G. A. Kelly, X. Li, K. Onogi, S. Saarinen, N. Sokka, R. P. Allan, E. Andersson, K. Arpe, M. A. Balmaseda, A. C. M. Beljaars, L. van de Berg, J. Bidlot, N. Bormann, S. Caires, F. Chevallier, A. Dethof, M. Dragosavac, M. Fisher, M. Fuentes, S. Hagemann, E. Holm, B. J. Hoskins, L. Isaksen, P. A. E. M. Janssen, R. Jenne, A. P. McNally, J.-F. Mahfouf, J.-J. Morcrette, N. A. Rayner, R. W. Saunders, P. Simon, A. Sterl, K. E. Trenberth, A. Untch, D. Vasiljevic, P. Viterbo, and J. Woollen (2005). The ERA-40 re-analysis. *Quart. J. Roy. Meteor. Soc. 131*, 2961–3012.

Wedi, N. P. (2004). Numerical simulation of internal gravity wave dynamcis. Proc. ECMWF Workshop on Recent Developments in numerical methods for atmosphere and ocean modelling, Reading, UK, pp. 221–232. Eur. Cent. For Medium-Range Weather Forecasts.

Wedi, N. P. (2006). The energetics of wave-driven mean flow oscillations. *Int. J. Numer. Methods Fluids 50*(10), 1175–1191. Special issue: Multidimensional Positive Definite Advection Transport Algorithm Methods.

Wedi, N. P. and P. K. Smolarkiewicz (2006). Direct numerical simulation of the Plumb-McEwan laboratory analog of the QBO. *J. Atmos. Sci. 63*(12), 3226–3252.

Wedi, N. P. and P. K. Smolarkiewicz (2009a). A framework for testing global nonhydrostatic models. *Q.J.R. Meteorol. Soc. 135*, 469–484.

Wedi, N. P. and P. K. Smolarkiewicz (2009b). A nonlinear perspective on the dynamics of the MJO: idealized large-eddy simulations. *J. Atmos. Sci.*. avail. online.

Wedi, N. P., K. Yessad, and A. Untch (2009). The nonhydrostatic global IFS/ARPEGE: model formulation and testing. Technical Report 594, Eur. Cent. For Medium-Range Weather Forecasts, Reading, UK.

Williamson, D. L., J. B. Drake, J. J. Hack, R. Jakob, and P. N. Swarztrauber (1992). A standard test set for numerical approximations to the shallow water equations in spherical geometry. *J. Comput. Phys. 102*, 211–224.